Chapter 6

Tilted to untilted phase transition in a mixed Langmuir monolayer

6.1 Introduction

Monolayer formation has been reported for hydrophobic oils which are weakly polar and mesogenic in nature [1]. Here the molecules possess a weak dipole moment at the center nearly perpendicular to the long molecular axis. The formation of monolayer in these materials was found to depend strongly on temperature. Their studies also indicate that a correlation exists between the spreading behavior of molecules at different temperatures and its bulk liquid crystalline phases. In the literature, for a monolayer, phase transition from a tilted state to untilted state has been reported for many mesogenic systems [2, 3]. In this chapter, we discuss on the mixed monolayer behavior of a weakly polar diheptylazoxybenzene(7AOB) with a strongly polar Octylcyanobiphenyl(8CB). It is interesting to probe the interactions between the flexible chains of 7AOB with rigid biphenyl core of 8CB. The 7AOB molecule possess a weak dipole moment which is nearly normal to its long molecular axis.

6.2 Experiment

The materials diheptylazoxybenzene and octylcyanobiphenyl (Aldrich) were procured commercially. The purity of them were checked by verifying the transition temperatures. The material 7AOB in the bulk exhibited the following phase sequence: Crystal – Smectic-A; 33.6°C, Smectic-A – Nematic; 53.4°C and Nematic – Isotropic; 70.4°C. The structure of

7AOB is shown in Figure 6.1. The central core consists of a weakly polar azoxy group. This weak azoxy dipole is nearly normal to the long molecular axis of 7AOB. The structure of 8CB has been described earlier in chapter-3. Here a strong cyano polar group is present along the molecular axis.

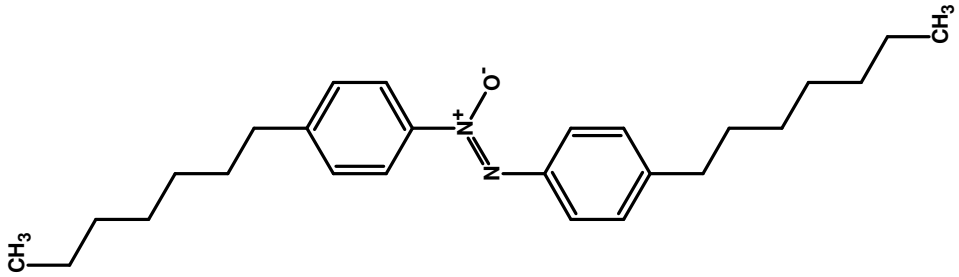

Figure 6.1: Structure of Diheptylazoxybenzene(7AOB)

We have carried out π - A/M experiments for 7AOB−8CB mixed system at 29±1 °C. Temperature was maintained constant by circulating the water using a thermostat. The setup for measuring isotherm has been described in detail in chapter-3. Stock solution of 1.5 mM concentration was used to prepare the mixtures. The compression rate was 0.9 (Å^2/molecule)/min. Epifluorescence and Brewster angle microscopy techniques were used to observe the monolayer phases. The experimental details of these techniques have been discussed in chapter-3 and chapter-5 respectively.

6.3 Results

The surface pressure(π)-area per molecule(A/M) isotherms carried out for 7AOB monolayer at different temperatures are shown in Figure 6.2. At 20 °C, for 7AOB, the surface pressure was almost zero at large A/M and it showed about 0.2 mN/m at 10 Å^2. At 30 °C, the surface pressure was less than 0.1 mN/m for A/M values higher than 26 Å^2. With compression, the surface pressure gradually increased upto an A/M of 18 Å^2. Below this A/M, a slope change was observed indicating a structural change in the monolayer. On further compression, the monolayer collapsed at 0.9 mN/m with a limiting area per molecule(A_0) of 18.4 Å^2. At 40 °C, the monolayer exhibited a collapse pressure, π_c, of 0.5 mN/m and an A_0 value of 26.7 Å^2.

The π-A/M isotherm and the monolayer phases for 8CB are described in detail in chapter-3.

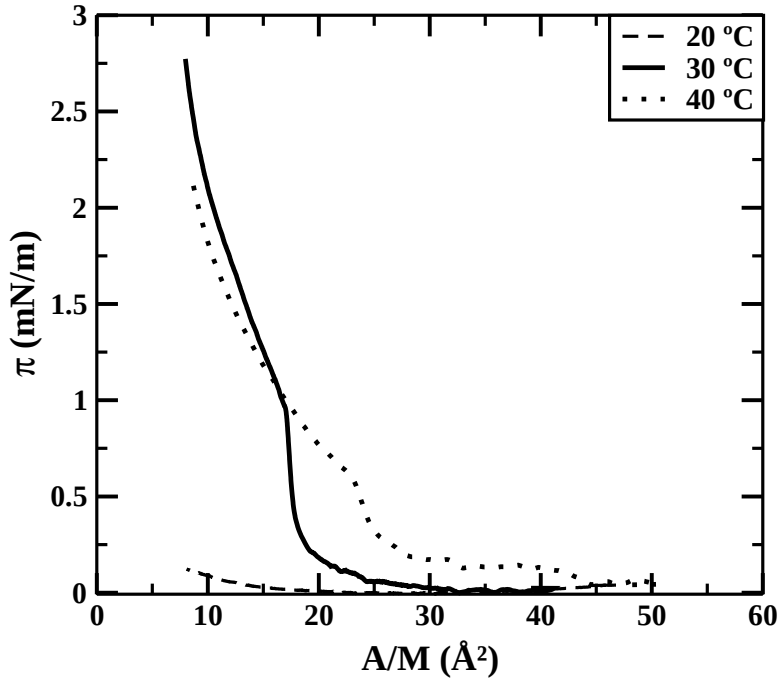

Figure 6.2: Surface pressure(π)-area per molecule(A/M) isotherms for 7AOB monolayer at different temperatures.

We have investigated the π-A/M isotherm at a temperature of 29 °C for the mixed monolayer of 7AOB and 8CB system at various compositions. This is shown in Figure 6.3. The 7AOB monolayer exhibits very low π_c of 0.7 mN/m and an A_0 value of 19 $Å^2$. At 0.5 MF of 7AOB in 8CB, an increase in the collapse pressure was seen when compared to that of 7AOB monolayer. Above an A/M value of 20 $Å^2$, the surface pressure was less than 0.1 mN/m. Upon compression, there was a slope change in the isotherm occurring at an A/M value of 19 $Å^2$. Thereafter, the surface pressure increased and terminated at a collapse pressure of 6.2 mN/m with an A_0 value of 17.7 $Å^2$. After the collapse, the surface pressure increased gradually and exhibited another kink. Careful analysis of the isotherm at 0.5 MF of 7AOB in 8CB showed an interesting feature revealing two changes in slope. This is shown in Figure 6.12. The first region spans the range from 18.5 $Å^2$ to 17.2 $Å^2$. The second region spanned from 17.2 $Å^2$ to 16.6 $Å^2$.

The presence of the kinks in the mixed monolayer phase became progressively clear at still lower concentrations of 7AOB. At 0.2 MF of 7AOB in 8CB, the surface pressure was

less than 0.1 mN/m above 41 $Å^2$. With compression, the surface pressure started to increase at 40 $Å^2$. Further compression led to a sharp slope change at 20 $Å^2$. The monolayer collapsed at surface pressure of 9 mN/m with an A_0 value of 19.6 $Å^2$. The surface pressure increased gradually after the collapse.

The isotherm for 0.1 MF of 7AOB in 8CB was similar to that of 8CB monolayer. However, the mixed monolayer collapsed at a lower surface pressure of 2 mN/m. This indicated that for even at low MF of 7AOB in 8CB, the 8CB monolayer gets destabilized.

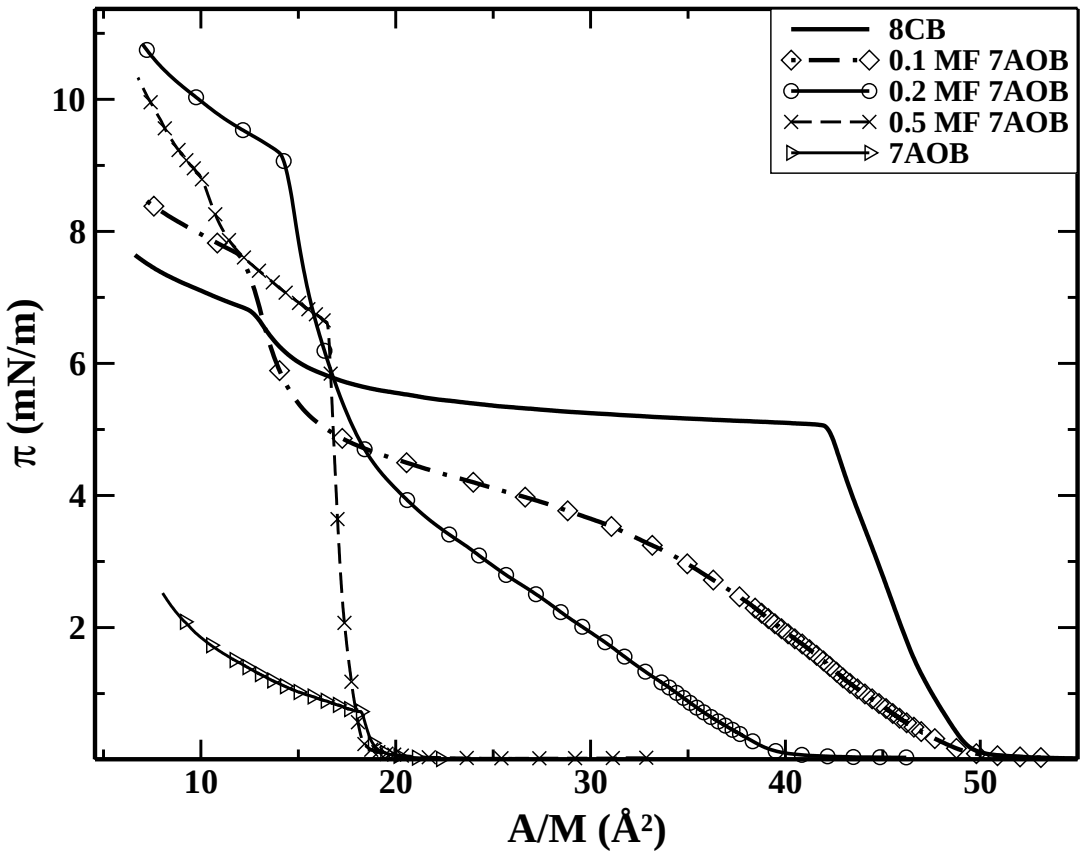

Figure 6.3: Surface pressure(π)-area per molecule(A/M) isotherms for different mole fraction (MF) of diheptylazoxybenzene(7AOB) in octylcyanobiphenyl(8CB) at 29 °C.

The variation of the collapse pressure with increasing mole fraction(MF) of 7AOB in 8CB is shown in Figure 6.4. In general, the collapse pressures of the mixed monolayer was higher than the individual monolayers except at extreme mole fractions. The collapse pressures of 8CB and 7AOB were 4.9 mN/m and 0.7 mN/m. A linear trend in the value of collapse pressure(π_c) for higher MF of 7AOB were observed which indicated a good

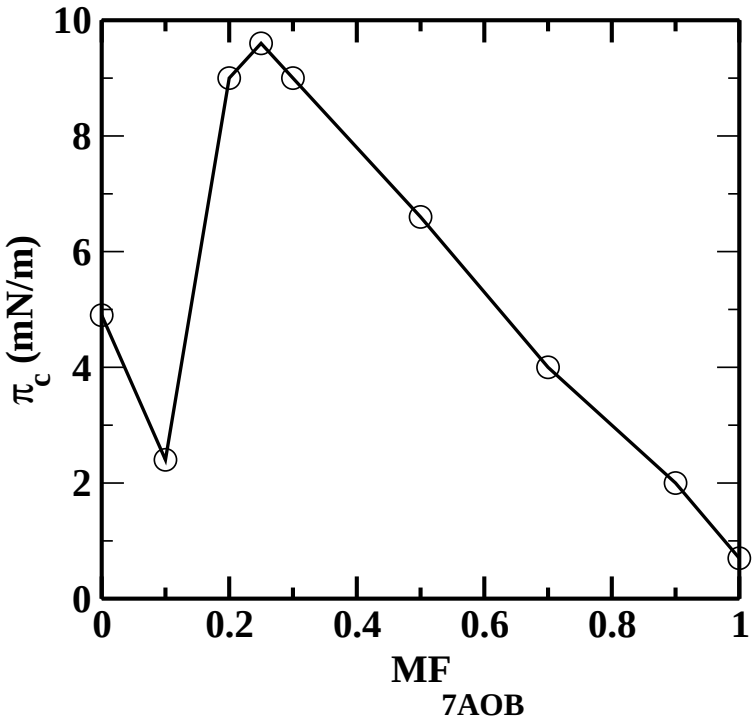

Figure 6.4: Variation of the collapse pressure, π_c, with increasing mole fraction(MF) of 7AOB in 8CB.

miscibility between the components.

We have carried out epifluorescence microscopy for the 7AOB−8CB mixed monolayer. The epifluorescence images for 7AOB monolayer are shown in Figure 6.5. At very large A/M, the monolayer exhibited gas(G) + L_1' coexisting phase(Figure 6.5(a)). The G phase appeared dark while L_1' phase appeared grey. With compression, L_1' phase was predominantly seen to coexist with traces of G phase(Figure 6.5(b)). Further compression led to the collapse of the mixed monolayer. Here brighter domains with varying intensities appeared indicating the onset of multilayers(Figure 6.5(c)). At still higher values of A/M, growth of larger multilayer domains were seen(Figure 6.5(d)).

The epifluorescence images for 0.5 MF of 7AOB in 8CB are shown in Figure 6.6. At large A/M, bright L_1 phase was seen to coexist with grey L_1' phase and the dark G phase(Figure 6.6(a)). With compression, the G domains tend to disappear leading to the coexistence of bright L_1 phase and grey L_1' phase(Figure 6.6(b)). Further compression led to the increase in the L_1' phase at the expense of L_1 phase (Figure 6.6(c)). At still lower A/M,

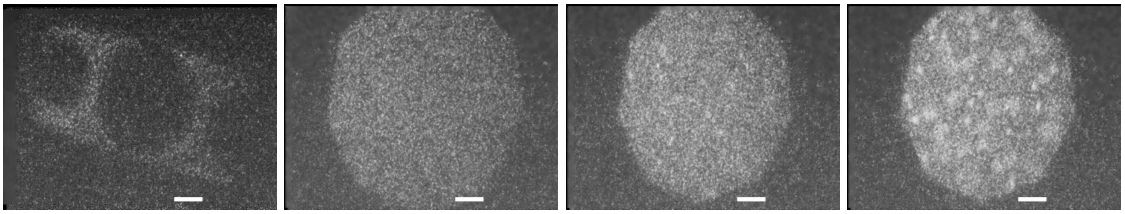

(a) 114.3 Å^2 (b) 19.9 Å^2 (c) 10.9 Å^2 (d) 6.2 Å^2

Figure 6.5: Epifluorescence images of 7AOB. Figure(a) represents G(dark) + L_1'(grey) phase. Figure(b) shows the presence of L_1' phase which appeared uniformly grey. Figure(c) shows the onset of multilayers coexisting with L_1' phase. Figure(d) shows the bigger multilayer domains coexisting with L_1' phase in the background. Scale bar represents 50 μm.

the two phase region disappeared and uniform L_1' phase was seen. The monolayer collapsed at low A/M. Here, still bright domains appeared which were multilayers coexisting with L_1' phase in the background(Figure 6.6(d)).

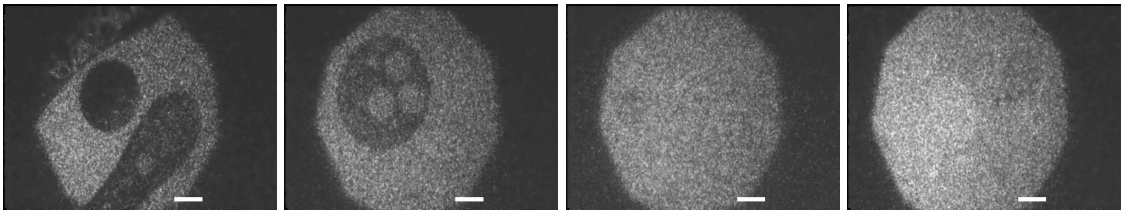

(a) 41.3 Å^2 (b) 21.4 Å^2 (c) 17.7 Å^2 (d) 6.3 Å^2

Figure 6.6: Epifluorescence images for 0.5 MF of 7AOB in 8CB. Figure(a) shows the presence of G + L_1(bright) phase with traces of L_1' phase. Figure(b) shows the presence of coexisting L_1(bright background) + L_1'(grey) phase. Figure(c) shows the predominantly present L_1' phase with traces of L_1 phase. Figure(d) shows the collapsed state. Here, the bright domains represent multilayers with L_1' phase in the background. Scale bar represents 50 μm.

The epifluorescence images for 0.2 MF of 7AOB in 8CB are shown in Figure 6.7. At large A/M, the coexisting G + L_1 + L_1' phases were seen(Figure 6.7(a)). Upon compression, the G(dark) domains disappeared showing the L_1(bright) and L_1'(grey) coexisting phases (Figure 6.7(b)). The L_1'(grey) phase grew more at the expense of L_1(bright) phase(Figure 6.7(c)). Further compression led to collapse. This is shown in Figure 6.7(d). Here the bright domains with varying intensities are multilayers coexisting with L_1' phase in the background.

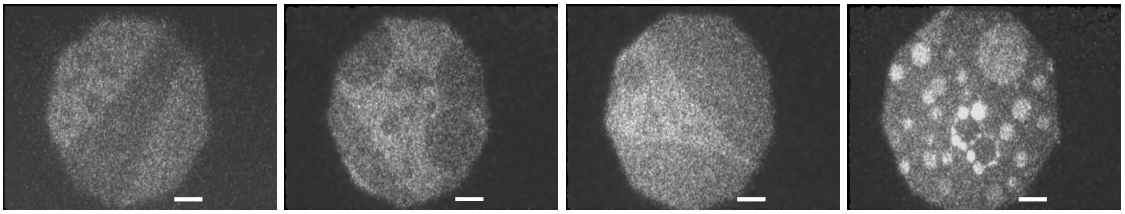

(a) 52.2 Å^2 (b) 24.3 Å^2 (c) 16.9 Å^2 (d) 8.4 Å^2

Figure 6.7: Epifluorescence images for 0.2 MF of 7AOB in 8CB. Figure(a) shows the coexistence of L_1 + L_1' phase with gas(dark) phase. Figure(b) shows the coexistence of L_1(bright) + L_1'(grey) phase. Figure(c) shows L_1'(grey) phase with relatively less L_1 phase. Figure(d) shows the collapsed state. Here the bright domains represents multilayers coexisting with L_1'(grey) phase in the background. Scale bar represents 50 μm.

The Brewster angle microscopy(BAM) images for 7AOB monolayer is shown in Figure 6.8. At very large A/M, circular *G*(dark) domains coexisted with L_1'(bright) phase(Figure 6.8(a)). With compression, L_1' phase appeared with some *G* domains(Figure 6.8(b)). After the collapse, small brighter domains appeared. These were multilayer domains which coexisted with $G + L_1'$ phase. We observed that the G domains did not vanish completely even after the collapse.

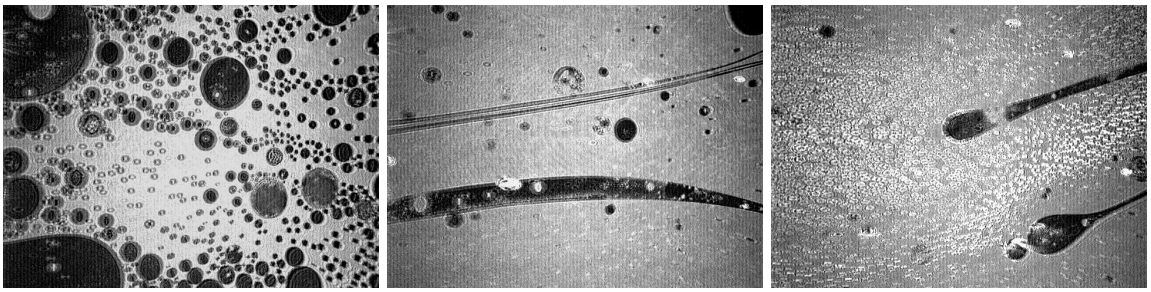

(a) 56.5 Å^2 (b) 22.1 Å^2 (c) 15.4 Å^2

Figure 6.8: Brewster angle microscopy images for 7AOB. Figure(a) shows the coexisting $G + L_1'$ phase. Figure(b) shows the predominantly present L_1' phase with some *G* domains. Figure(c) shows the collapsed state. Here the small bright domains were multilayers which coexist with L_1' phase and *G* phase. Scale of each image is 6.4 x 4.8 mm^2.

The BAM images for 0.5 MF of 7AOB in 8CB are shown in Figure 6.9. Interestingly for this composition, a different behavior was observed. At very large A/M, we find three different coexisting phases. They were, *G*(dark) + L_1'(bright) and L_1(grey) phases. We identify

L_1' phase as compactly packed and L_1 phase as loosely packed phase based on the difference in their contrasts under BAM and epifluorescence and from the π-A/M isotherms. These phases are seen in Figure 6.9(a). With compression, the G domains disappeared in size with L_1' phase coexisting with L_1 and G phase (Figure 6.9(b)). Further compression led to the collapsed state. Here, L_1' phase was seen to coexist with the multilayer phase(Figure 6.9(c)). At still lower A/M, multilayer domains increased in size. These multilayer domains were much brighter than the L_1' or L_1 phase(Figure 6.9(d)).

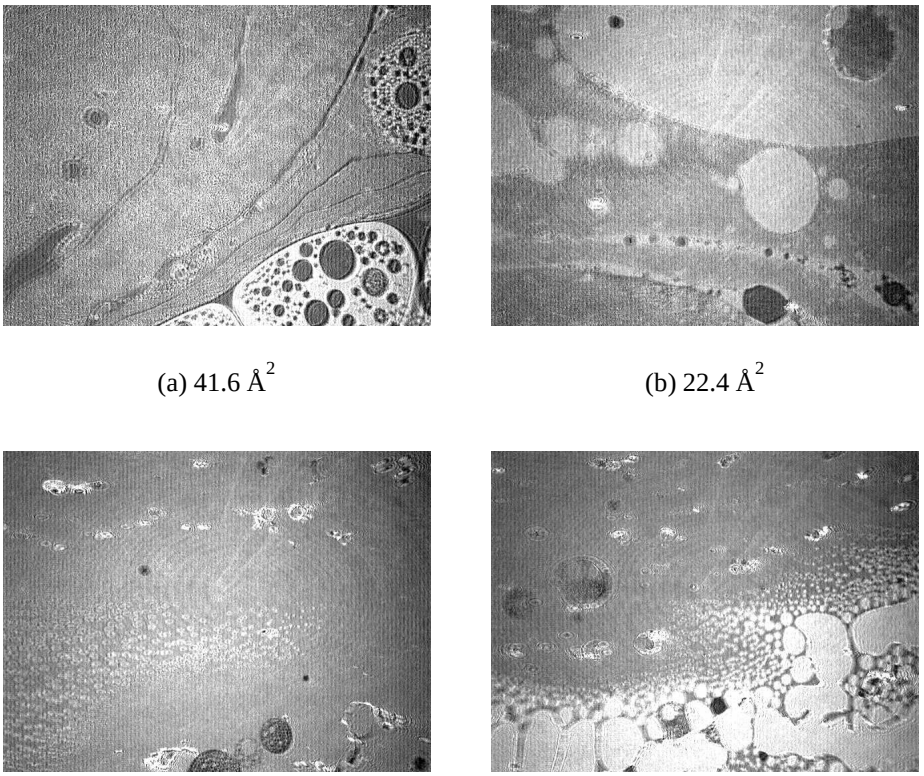

(a) 41.6 Å^2 (b) 22.4 Å^2

(c) 18.9 Å^2 (d) 16 Å^2

Figure 6.9: Brewster angle microscopy images for 0.5 MF of 7AOB in 8CB. Figure(a) shows the coexisting G(dark) + L_1(grey) + L_1'(bright) phase. Figure(b) shows the L_1'(grey) phase coexisting with L_1(bright) phase with G(dark) phase. Figure(c) shows the collapsed state. Here, the predominantly present L_1' phase coexist with traces of multilayer domains(brighter) and G phase. Figure(d) shows the presence of multilayers coexisting with L_1' phase in the background. Scale of each image is 6.4 x 4.8 mm^2.

The BAM images for 0.2 MF of 7AOB in 8CB are shown in Figure 6.10. At very large A/M, we could see the presence of G(dark) domains coexisting with L_1(grey background)

phase. The G domains showed fingering patterns(Figure 6.10(a)). With compression, L_1' phase was seen to grow at the expense of L_1 phase (Figures 6.10(b) and 6.10(c)). Further compression led to collapsed state. Here, bright multilayers were seen to coexist with L_1' phase.

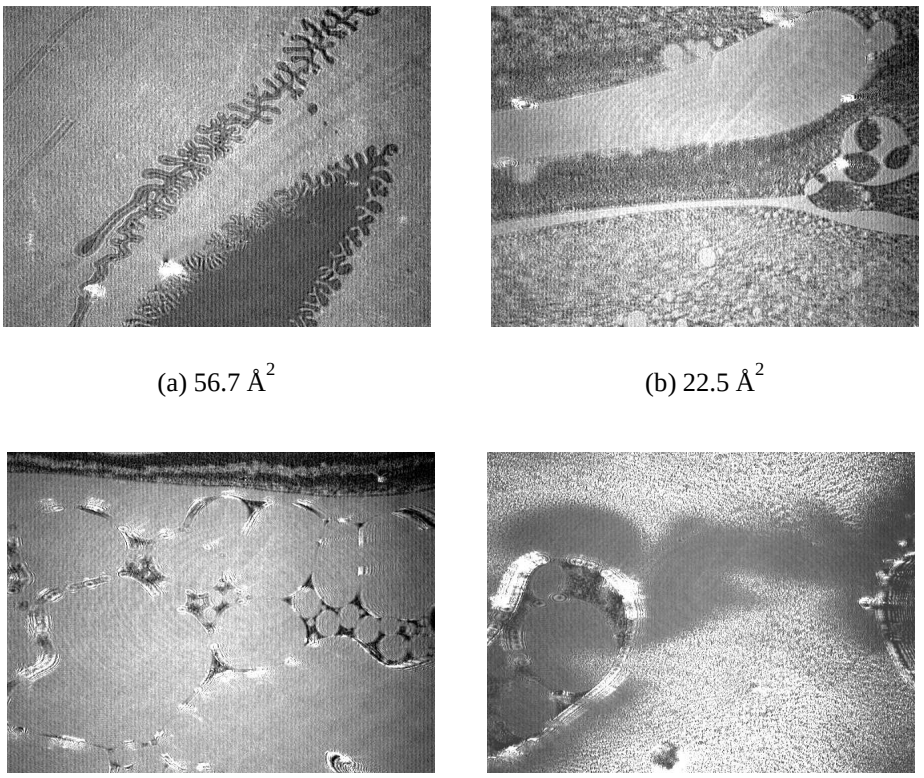

(a) 56.7 Å^2 (b) 22.5 Å^2

(c) 16.6 Å^2 (d) 12.7 Å^2

Figure 6.10: Brewster angle microscopy images for 0.2 MF of 7AOB in 8CB. Figure(a) shows coexisting G(dark) + L_1(grey) phase. Here, a fingering pattern of G phase is seen. Figure(b) shows the coexistence of L_1'(bright) phase and L_1(grey) phase. Figure(c) shows the predominant L_1' phase coexisting with traces of L_1 phase in the background. Figure(d) shows the collapsed state. Here the bright dots are multilayers which coexist with L_1' phase. Scale of each image is 6.4 x 4.8 mm^2.

6.4 Discussions

We have investigated the mixed monolayer of 7AOB and 8CB using surface manometry, epifluorescence and Brewster angle microscopy techniques. We find the nature of the π-A/M isotherm for 7AOB depends strongly on temperature. The spreading of the monolayer

showed a correlation with its bulk liquid crystalline transition temperatures. With increasing temperature, the limiting A/M, A_0, tends to shift to higher A/M. At 20 °C, there was no stable monolayer. At 30 °C, the monolayer was stable with an A_0 value of 18.4 $Å^2$ and collapsed at a surface pressure of 0.9 mN/m. At 40 °C, the monolayer was still stable with an A_0 value of 26.7 $Å^2$ but exhibited comparatively a lower collapse pressure of 0.5 mN/m. At 20 °C, 7AOB material in the bulk exhibits crystalline state which does not favor the formation of a stable monolayer. However, at 30 °C and 40 °C, the material exhibits smectic phase which favors the formation of stable monolayer as shown by our π-A/M isotherm studies. At still higher temperature, the material exhibits nematic phase and we find that it forms a monolayer with still lower collapse pressure. This shows that the monolayer formation was not very favorable in the nematic phase compared to smectic phase. Such spreading behavior of monolayer that depends strongly on its bulk liquid crystalline transition temperatures has been reported for weakly polar(hydrophobic oils) materials [1]. These materials exhibited liquid-condensed phase at the A-W interface at a temperature corresponding to their bulk liquid crystalline phase. The reason for the stability of this weakly polar monolayers was attributed to entropic origin due to dispersive forces between the chains and the aromatic cores. This appears to be the mechanism for the formation of monolayer in 7AOB.

The 8CB monolayer which is tilted to about 60° from the surface normal gives rise to an L_1 phase where the tilt azimuth is isotropic [4, 5]. The tilt is caused due to dipole-dipole repulsions between the polar head groups leading to an A/M of 48 $Å^2$. Our surface manometry and microscopy experiments on 8CB show the phase sequence: $G + L_1$, L_1, $L_1 + D_1$ and $L_1 + D_1 + D_2$ domains. These are in agreements with other reports [6, 7, 8]. Maxwell displacement current and second harmonic generation studies on 8CB monolayer report a transition(at very large A/M) from planar isotropic phase to a tilted phase on compression [5].

Our surface manometry on the mixed monolayer of 7AOB and 8CB shows a linear trend in the collapse pressure except at extreme compositions(Figure 6.4). The maximum stability for the mixed monolayer occurred at 0.25 MF of 7AOB in 8CB. Here, the collapse

pressure(π_c) was 9.6 mN/m. For the compositions ranging from 0.2 MF to 0.7 MF of 7AOB in 8CB, the mixed monolayer exhibited two slope changes below the collapse. This indicated a phase transition in the mixed monolayer. The slope changes were clearer at 0.2 MF of 7AOB in 8CB(Figure 6.3). The epifluorescence studies on the individual 7AOB monolayer indicated the phase sequence: $G + L_1'$, L_1' and L_1' + multilayers (Figure 6.5). The phase sequences of 8CB are, $G + L_1$, L_1, L_1 + three layer(D_1) and $L_1 + D_1$ + multilayer(D_2) phases. The L_1' phase of 7AOB monolayer appeared grey than the L_1 phase of 8CB monolayer. The mixed monolayer of 7AOB−8CB system showed an interesting behavior. It exhibited two different monolayer phases coexisting with G phase for the compositions ranging from 0.2 MF to 0.7 MF of 7AOB in 8CB. In the mixed monolayer, we assign, the monolayer phase which was more fluidic and brighter under epifluorescence as L_1 phase. The other phase which appeared grey and less fluidic was assigned as L_1' phase. The coexisting $G + L_1 + L_1'$ phases on compression transformed to L_1 and L_1' coexisting phase. Further compression, led to the formation of L_1'(grey) phase. At lower A/M, the L_1' phase transformed to multilayers. This phase sequence was clearly seen for 0.2 MF of 7AOB in 8CB in the mixed monolayer (Figures 6.7(b) and 6.7(c)).

We have also carried out BAM studies on these mixed monolayer systems to confirm the observed phases. The BAM images for L_1 phase appeared grey and that of L_1' phase appeared more bright. The BAM images for 0.5 MF of 7AOB in 8CB are shown in Figure 6.9. The L_1' phase which appeared grey in the epifluorescence appeared more bright in the BAM images. The L_1 phase which appeared more bright under epifluorescence appeared grey under BAM images. This can be interpreted as the L_1 phase is loosely packed and L_1' phase is compactly packed. Thus in epifluorescence the dye gets easily dispersed in L_1 phase causing it to appear bright when compared to L_1' phase. On the other hand, in the BAM images the intensity reflects the ordering of the molecules. Thus the compactly packed L_1' phase appeared bright compared to L_1 phase. The general trend seen in both epifluorescence and BAM methods were the transformation of the $L_1 + L_1'$ phase to L_1' phase. We find that this transformation occurs for 20% of 7AOB in 8CB mixed monolayer.

The rigidity of the mixed monolayer was ascertained by calculating the elastic modulus. The compressional elastic modulus, $|E|$, was calculated using,

$$|E| = (A/M)d\pi/d(A/M) \tag{6.1}$$

The variation of $|E|$ with A/M for 7AOB monolayer is shown in Figure 6.11. The $|E|$ showed a maximum value of 20.6 mN/m at an A/M of 18.6 $Å^2$. For 8CB monolayer, the maximum value of $|E|$ was calculated to be 35.8 mN/m at an A/M of 45.6 $Å^2$. The variation of $|E|$ with

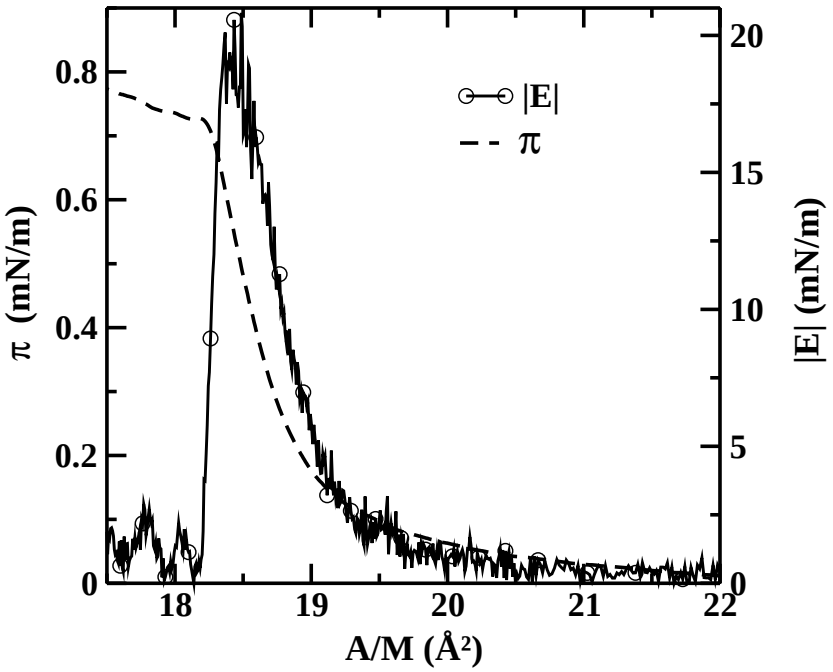

Figure 6.11: Variation of the compressional elastic modulus, $|E|$, and the surface pressure, π with A/M for 7AOB. The continuous lines with circles, represent $|E|$ and the dashed lines represent π. The vertical axis on the left gives the scale for π and the vertical axis on the right gives the scale for $|E|$.

A/M at 0.5 MF of 7AOB in 8CB is shown in Figure 6.12. The maximum value of $|E|$ for 0.5 MF of 7AOB in 8CB was 110 mN/m at 16.8 $Å^2$. The $|E|$ value of the mixed monolayer was larger than the individual monolayers showing a much better stability in the mixture. We find a sharp change in the value of $|E|$ at an A/M of 17.5 $Å^2$ indicating a phase transition. It is interesting to see that the phase below an A/M of 17.5 $Å^2$ has much higher value of $|E|$ compared to the phase above this A/M. We infer from these studies that the phase transition is from a loosely packed mixed monolayer to a compactly packed mixed monolayer. It is

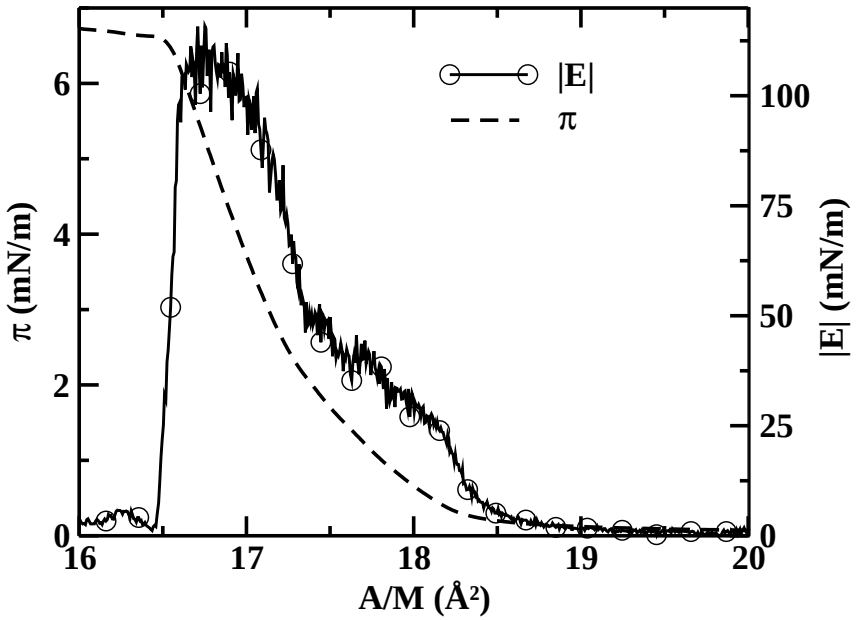

Figure 6.12: Variation of the compressional elastic modulus, $|E|$, and the surface pressure, π with A/M at 0.5 MF of 7AOB in 8CB. The continuous lines with circles, represent $|E|$ and the dashed lines represent π. The vertical axis on the left gives the scale for π and the vertical axis on the right gives the scale for $|E|$.

known that the 8CB molecules are tilted at an angle of 60° and are loosely packed. Thus we attribute the observed transition induced by compression to change in orientation of 8CB molecules from the tilted state to untilted state in the mixed monolayer. i.e. from $L_1 + L_1'$ coexisting phase to L_1' phase. This model is consistent with the different intensity patterns in L_1 and L_1' phases seen under epifluorescence and BAM studies. From these analyses, we can arrive at the conclusion that L_1 phase which is characteristic of 8CB molecules is a tilted phase and the L_1' phase which is characteristic of 7AOB is an untilted phase. In the mixed monolayer, the $L_1 + L_1'$ coexisting phase undergoes a phase transition to L_1'(untilted) phase.

Based on these results, a phase diagram was constructed for the 7AOB-8CB mixed monolayer. This is shown in Figure 6.13. The monolayer behaved as that of individual components at the extreme mole fractions. For intermediate compositions of 8CB, around 0.2 MF to 0.9 MF of 7AOB in 8CB, we find a coexisting $G + L_1 + L_1'$ phase. At low A/M, this transformed to $L_1 + L_1'$ coexisting phase. At still lower A/M, the $L_1 + L_1'$ coexisting phase transformed to L_1' phase which collapsed to multilayers with background as L_1' phase.

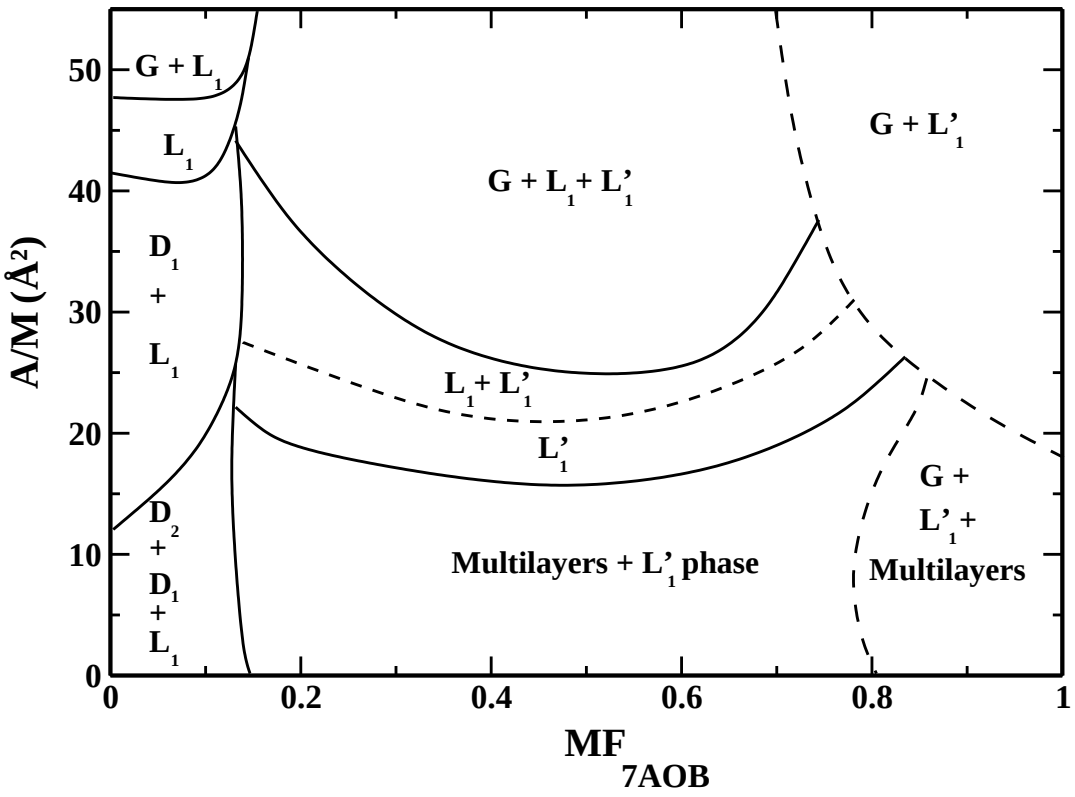

Figure 6.13: Phase diagram of the 7AOB-8CB mixed monolayer at t=29 °C. Here, the continuous lines indicate the actual phase boundaries and the dashed lines indicate the approximate phase boundaries.

To summarize, we have found a orientational phase transition from a tilted loosely packed L_1 phase to untilted compactly packed L_1' phase in 7AOB-8CB mixed monolayer system. The presence of 7AOB in smaller concentrations was sufficient to bring the transition to the untilted, anisotropic, ordered liquid phase from the tilted disordered liquid phase. Based on these studies, we correlate the formation of the untilted and more ordered phase to the reduction of the repulsive dipole-dipole interactions between 8CB molecules by the presence of flexible alkyl chains of 7AOB. It might be possible that the presence of rigid biphenyl core of 8CB freezes the flexibility of alkyl chains of 7AOB thereby bringing in the condensation. The interplay between entropic and energetic interactions lead to the occurrence of the untilted phase. These phase transitions from tilted to untilted state are gaining more attention both theoretically and experimentally [5], [9, 10, 11]. We hope our results to provide more insight in understanding them.

Bibliography

[1] Y. Tabe, T. Yamamoto, I. Nishiyama, K.M. Aoki, M. Yoneya and H. Yokoyama, Jour. Phys. Chem. B., **106**, 12089, 2002.

[2] M. Iwamoto and Z. Ou-Yang, Jour. Chem. Phys., **117**, 7705, 2002.

[3] A. Tojima, T. Manaka and M. Iwamoto, Jour. Chem. Phys., **115**, 9010, 2001.

[4] J. Xue, C.S. Jung and M.W. Kim, Phys. Rev. Lett., **69**, 474, 1992.

[5] A. Tojima, T. Manaka, M. Iwamoto and O. Zhong-can, Jour. Chem. Phys., **118**, 5640, 2003.

[6] M.C. Friedenberg, G.G. Fuller, C.W. Frank and C.R. Robertson, Langmuir, **10**, 1251, 1994.

[7] N.G.M.D. Mul and J.A. Mann Jr., Langmuir, **10**, 2311, 1994.

[8] K.A. Suresh and A. Bhattacharyya, Langmuir, **13**, 1377, 1997.

[9] A. Sugimura, M. Iwamoto and O. Zhong-can, Phys. Rev. E., **50**, 614, 1994.

[10] S. Shin and S.A. Rice, Jour. Chem. Phys., **101**, 2508, 1994.

[11] S. Karaborni and S. Toxevaerd, Jour. Chem. Phys., **97**, 5876, 1992.